JCTC Journal of Chemical Theory and Computation

Capturing the Trans Influence in Low-Spin d^8 Square-Planar Platinum(II) Systems using Molecular Mechanics

Anna. E. Anastasi and Robert J. Deeth*

Inorganic Computational Chemistry Group, Department of Chemistry, University of Warwick, Coventry CV4 7AL, U.K.

Received April 1, 2009

Abstract: Molecular modeling of coordination complexes continues to present challenges for force field methods. Implicit or explicit treatment of the significant d electron effects is mandatory. Ligand field molecular mechanics is designed for coordination complexes by explicitly including the ligand field stabilization energy (LFSE) and it is applied here to model the trans influence in tetracoordinate Pt^{II} complexes of general formulas PtX_4, PtX_3Y, *cis*-PtX_2Y_2, and *trans*-PtX_2Y_2, where X and Y are OH_2, H^-, Cl^-, Br^-, PR_3, SH_2, NR_3, and pyridine. Parameters have been developed within the Merck molecular force field using DFT structures and energies as reference data. Both geometric changes and relative energies are generally well-reproduced although PH_3 and H^- complexes show deviations. However, for phosphine complexes, replacing PH_3 with PMe_3 resolves all bar one of these. The LFSE associated with the low-spin d^8 configuration ensures planar coordination and provides an electronic connection between all the ligands, thus enabling a correct description of the trans influence. The parameters developed for NR_3 and PR_3 with R = H work well for R = Me and Et and, in agreement with experimental and/or DFT structures, display either a tetrahedral distortion or even ligand dissociation.

Introduction

The trans influence was first defined by Pidcock et al. in 1966[1] as "the extent to which a ligand weakens the bond trans to itself in the equilibrium state of a substrate". Trans influences manifest as changes in metal−ligand (M−L) bond lengths, IR frequencies, and/or NMR chemical shifts and are routinely observed in transition metal complexes, particularly planar platinum(II) species.

One of the earliest studies[2] compared Pt^{II}−Cl bond lengths in a number of complexes and proposed the following trans influence series: $R_3Si^- > H^- > PR_3 > C{=}C$, $Cl^- > O(acac)$. The larger trans influence correlates with increased metal−ligand covalency. The series has since been significantly extended.

Pearson rationalized the trans influence in terms of "antisymbiosis".[3] Over a decade earlier, Jorgensen had defined "symbiosis" as the tendency of a hard base to retain its electrons, thus keeping the attached metal hard, too.[4] Conversely, a soft base will transfer charge to the metal, making it soft. Antisymbiosis is the opposite: a hard base bonded to a central atom encourages coordination from a soft base and vice versa.

In molecular orbital terms, the trans influence is most often described as a competition between the two trans ligands for a single, metal-based orbital. One ligand donating strongly into this (initially empty) orbital effectively pre-empts the other, leading to a relative weakening of the latter's bonding. The metal orbital is generally regarded as an sd hybrid utilizing the highest-energy metal d orbital, which, in planar d^8 complexes and assuming the *x* and *y* axes lie long the Pt−L bonds, corresponds to $d_{x^2-y^2}$.[5] Thus, the trans influence is dominated by M−L σ-bonding.[1]

Alternatively, the trans influence can be rationalized by hypervalent valence bond theory.[6] Here, the contribution from the two resonance structures depends on the abilities of X: and Y: to support the lone pair.

* To whom correspondence should be addressed. E-mail: r.j.deeth@warwick.ac.uk. Website: http://warwick.ac.uk/go/iccg.

10.1021/ct9001569 CCC: $40.75
Published on Web 08/20/2009

$$X{:}Pt{-}Y \leftrightarrow X{-}Pt{:}Y$$

Thus, if Y is electronegative and (isolated) Y: is relatively stable, the right-hand structure is favored and the X−Pt bond is short.

The mutual interplay between ligands on opposite sides of the coordination center is clearly an electronic effect. Hence, quantitative theoretical descriptions of the trans influence have largely been based on quantum chemical methods like density functional theory (DFT). However, while DFT has clearly revolutionized the application of quantum mechanics (QM) in transition metal chemistry, current functionals are still not perfect. In addition, DFT is compute-intensive and therefore relatively slow.

In contrast, classical molecular mechanics (MM) is much faster, but conventional MM does not explicitly account for d electron effects and thus may not be generally suited to handle transition-metal complexes. We have therefore developed ligand field molecular mechanics (LFMM), which includes the ligand field stabilization energy (LFSE) directly.[7] LFMM thus describes the metal−ligand coordination better and can deliver DFT-quality results but up to 4 orders of magnitude faster.

Previous applications of LFMM have spanned Jahn-Teller effects in Cu(II) complexes[8,9] and spin state energetics of simple Co(III) species.[10] Here, we present our first complete attempt to describe the trans influence by modeling tetracoordinate Pt^{II} complexes of general formulas PtX_4, PtX_3Y, *cis*-PtX_2Y_2, and *trans*-PtX_2Y_2, where X and Y are OH_2, H^-, Cl^-, Br^-, PR_3, SH_2, NR_3, and pyridine. Since experimental data are available for only a few of the possible complexes, we compare the LFMM results with DFT structures and energies. The LFMM provides a satisfactory description of both the trans influence in $[PtX_3Y]^n$ systems and the relative energies of cis and trans forms of $[PtX_2Y_2]^m$.

Computational Details

Quantum Mechanical Calculations. Density functional optimizations were carried out using the Amsterdam Density Functional suite of programs (version 2006.01).[11] Structures were preoptimized using the local density approximation with a triple-ζ plus polarization basis set (TZP) on all atoms and a scalar ZORA relativistic correction.[12−14] Structures were then fully optimized using a gradient corrected functional, as described later, and include solvent effects based on the conductor-like screening model (COSMO) implemented in ADF.[15] COSMO radii were taken from Allinger's MM3 force field scaled by 0.833.[16,17] Frequencies were calculated numerically.[18,19]

QM charges were computed via the CHelpG method. To maintain compatibility with the way partial atomic charges are implemented in MMFF94, the Hartree−Fock approximation (as apposed to DFT) was used, as implemented in Gaussian 03[20] with 6-31G(d) basis sets on the nonmetal atoms. The LanL2DZ basis set with an extra set of f functions using the exponents determined by Frenking et al. and the accompanying frozen core were used for Pt.[21] Gaussian 03 only has van der Waals radii for elements up to Ar. In the AMBER charge scheme, and in GAMESS-US, heavier atoms are given a radius of 1.8 Å and we have followed this example. Bromine is given a radius of 2.3 Å, also consistent with the GAMESS-US approach.

Table 1. Pt−L Bond Charge Increments

ligand type	bci
OH2	0.2747
N	0.4121
NPYD	0.5531
CL-	0.3631
BR-	0.3939
HYDR	0.4347
S	0.5064
P	0.6683

Molecular Mechanics Parameters. The ligand field molecular mechanics (LFMM) treatment of charges was based on the MMF94 force field.[22] MMFF94 partial atomic charges employ the bond charge increment (bci) scheme, where the base charge q on an atom is modified by the bci value of each attached atom. New bci values for the metal, M, and the ligand donor atoms, L, were determined as follows. The bci for L is a quarter of the decrease in the QM-calculated Pt charge but then scaled relative to the ratio of the QM and LFMM proton charges for HL^+.[23]

Thus, the new bcis are given by

$$\mathrm{bci(L)} = 1/4\Delta q_{\mathrm{Pt}}^{\mathrm{MM}}(\mathrm{PtL_4}) = 1/4\Delta q_{\mathrm{Pt}}^{\mathrm{QM}}(\mathrm{PtL_4})\left(\frac{\Delta q_{\mathrm{H}}^{\mathrm{MM}}(\mathrm{HL^+})}{\Delta q_{\mathrm{H}}^{\mathrm{QM}}(\mathrm{HL^+})}\right)$$

where $\Delta q_{\mathrm{H}}^{\mathrm{MM}}(HL^+)$ is the change in proton charge of the protonated ligand as given by MMFF, $\Delta q_{Pt}^{QM}(PtL_4)$ is the change in the CHelpG Pt^{2+} charge for a $[PtL_4]$ complex, and $\Delta q_{\mathrm{H}}^{\mathrm{QM}}(HL^+)$ is the change in charge on H^+ for a protonated L. The final bci values are collected in Table 1.

In addition to the standard MMFF94 parameters, additional LFMM-specific parameters are required. In particular, and as described elsewhere,[24] the ligand field stabilization energy (LFSE) term is defined in terms of angular overlap model (AOM) parameters e_σ, $e_{\pi x}$, $e_{\pi y}$, and e_{ds}; the M−L stretch employs a Morse function while the angular geometry about the metal center is described via a ligand−ligand repulsion term. LFMM geometry optimizations employed Dommi-MOE,[24] our extended version of the Molecular Operating Environment.[25]

The AOM parameters, e_λ, were estimated by fitting the appropriate expressions to DFT "d" orbital energies from a "spherical configuration" calculation based on the DFT-optimized homoleptic structure. For d^8 Pt(II) species, this involves assigning the molecular orbitals of mainly Pt d parentage equal occupancies of 1.6. For planar PtL_4 systems, the d-orbital splitting yields three degrees of freedom and there are at most three AOM parameters assuming $e_{\pi x} = e_{\pi y}$. The Morse and ligand−ligand repulsion parameters were then roughly optimized using the penalty function approach proposed by Norrby and co-workers,[26] with the DFT-optimized geometries and selected frequencies as target data. All parameters were then further manually refined to give appropriate geometries for mixed ligand complexes. Full

listings of the LFMM parameters are available in the Supporting Information.

Results and Discussion

Despite the absence of an explicit LFSE term, conventional MM has been applied to the trans influence in planar d^8 systems. However, some intervention by the user may be necessary. For example, Rappé et al. have included Pt^{II} parameters in their universal force field.[27] The necessary trans coupling is achieved by varying the bond order of some ligands; for example, carbonyls are generally given a bond order of 2, but if they are trans to a ligand with a high trans influence then a reduced order of $1^1/_2$ is used. For metal−phosphine bonds, the bond order of the M−P bond is varied depending on whether a trans influence should be present.

A generalization of this approach appeared during the course of our study. An extended version of VALBOND,[28] VALBOND-TRANS,[29] incorporates Landis's hypervalence ideas such that the "normal" VALBOND parameters are modified to include contributions from both the ligand and its trans partner. VALBOND-TRANS was applied to octahedral organometallic compounds relevant to various catalytic processes and shows good agreement with DFT and experimental data. However, VALBOND-TRANS explicitly modifies the parameters to reflect the molecule and does not treat deviations in the A−M−B angle from 180°.

Another way of achieving the trans influence is to include a direct ligand−ligand distance term, which spans the intervening metal center. We made a preliminary investigation on model Pt complexes using an early form of LFMM[30] but did not take it any further. The following year, Brandt et al.[31] provided a more complete application of this approach to a series of six-coordinate Ru(II)−polypyridyl complexes, demonstrating that trans influences could be successfully treated with an additional, explicit N−N distance term. In contrast, LFMM tries to capture the trans influence implicitly and makes no assumption that the trans ligands must define a bond angle of 180° at the metal.

Another important feature of planar d^8 systems is their planarity. Landis and co-workers use a Fourier angular potential energy term to accommodate both 90° and 180° L−M−L bond angles in planar Rh(I) complexes,[32] while Cundari et al. have extended their MM2 force field to include three Pt−L atom types (where L = Cl^-, NR_3, CO_2^-) and enforce the planarity of Pt^{II} by including a lone pair on the + and − directions along the *z*-axis.[33] They report some success with their method, with average rms Pt−L differences of 0.08 ± 0.05 Å. However, they generally look at cis complexes and do not assess whether their method is also suitable for trans complexes.

The planar structure associated with the low-spin d^8 configuration can also be rationalized in terms of the LFSE. We have already shown that LFMM automatically generates the correct planar structures for low-spin four-coordinate Ni(II) amine complexes.[34] The observation that the trans influence involves metal-based sd hybrids interacting with ligand orbitals led us to wonder whether the treatment of sd^n hybridization implicit in the angular overlap model (AOM) d−s mixing term included in our model would provide a basis for capturing the trans influence as well.

Choice of Functional. The DFT structures and energies form the target data for the LFMM parameter optimization. Several X-ray crystal structures are available for $[PtCl_4]^{2-}$ in the Cambridge Structural Database, which we access via the EPSRC Chemical Database Service.[35] These provide a reliable estimate of the Pt−Cl distance of 2.30 ± 0.01 Å. We used this value in a preliminary screen of a range of functional/relativistic corrections/solvation combinations (see Supporting Information, Table S1) and eliminated those that gave an error greater than 0.12 Å. At this stage, it was clear that COSMO and relativistic corrections are important, but a range of common functionals survive.

Applying the same selection criterion to $[PtBr_4]^{2-}$ removes all the gradient-corrected functionals except OPBE (Supporting Information, Table S2). The computed Pt−N distances in $[Pt(NH_3)_4]^{2+}$ display a much smaller spread than either halide complex, and the gradient-corrected functionals, including OPBE, all give bond lengths within 0.03 Å of the experimental value of 2.05 Å (Supporting Information, Table S3). As a final test of the OPBE functional, the structures of *cis*- and *trans*-$[PtCl_2(NH_3)_2]$ were compared (Supporting Information, Table S4). The OPBE functional continues to provide a good description of the structure as well as predict that the trans isomer should be more stable than cis. Our favored DFT protocol is therefore OPBE/TZP/ZORA/COSMO.

The structures of all the homoleptic species were therefore optimized at the OPBE/TZP/ZORA level with a COSMO correction to model condensed phase effects.[36] Where more than one orientation of a ligand was possible, e.g., for $[Pt(OH_2)_4]^{2+}$, several geometries were optimized and the lowest energy one was used as the target geometry for the LFMM parameters. All possible ligand combinations of PtX_nY_{4-n} were optimized and added to the set of the target structures. Note that throughout the following the total charge is, for convenience, omitted from the molecular formulas.

A summary of results comparing geometries and energies from DFT and LFMM calculations is presented below.

In evaluating the LFMM data we consider several features: (1) the extent to which some Pt−L bonds change relative to their values in the homoleptic species, (2) the relative cis and trans Pt−X distances for species of the formulas PtX_3Y and the relative Pt−X and Pt−Y distances for both isomers of PtX_2Y_2, and (3) the relative energy of cis and trans PtX_2Y_2 isomers.

PtX_4. The final LFMM parameters utilized the whole target data set of homoleptic and mixed ligand species. Thus, and as shown in Table 2, there are some small discrepancies between the DFT and LFMM Pt−L bond lengths for the former group of complexes. If we had only wanted to study homoleptic systems, obtaining perfect agreement for them would have been trivial.

PtX_3Y. Defining how well LFMM treats the trans influence requires modeling of mixed-ligand systems. In complexes with the formula PtX_3Y we consider two features: (a) the difference between cis and trans Pt−X bond lengths

Table 2. Pt−L Bond Lengths (Å) for DFT- and LFMM-Optimized Geometries of Homoleptic [PtL_4] Species

	Pt-X		
X	DFT	LFMM	Δ(LFMM − DFT)
H^-	1.646	1.594	−0.052
Cl^-	2.310	2.333	0.023
Br^-	2.459	2.459	0.000
NH_3	2.035	2.047	0.012
OH_2	2.024	2.065	0.041
SH_2	2.307	2.290	−0.017
py	2.019	2.029	0.010
PH_3	2.325	2.299	−0.026

and (b) how much the Pt−Y bond length has changed in comparison to the homoleptic species.

Property a is particularly important, as it shows that we can distinguish between cis and trans ligands and correctly mimic the trans influence.

Figure 1 shows the difference between cis and trans Pt−Cl bond lengths in $PtCl_3X$ (mauve). The DFT and LFMM values agree to 0.018 Å or better, and in virtually all instances, the signs of the cis−trans Pt−Cl differences are the same. For those cases where the signs differ (Y = NH_3 or py), the magnitudes of the difference are less than the tolerance in computed bond lengths, i.e., about 0.02 Å. Hence, the cis and trans Pt−Cl distances are essentially the same for Y = Br, NH_3, SH_2, and py, while $Pt-Cl_{trans}$ is greatly lengthened for Y = H, moderately lengthened for Y = PH_3, and moderately shortened for Y = OH_2.

The LFMM description of the Pt−Cl bonds in [$Pt^{II}Cl_3Y$] species is very good. However, large cis−trans Pt−Cl differences are expected to be accompanied by corresponding changes in Pt−Y distance relative to the Pt−Y bond length in the relevant homoleptic system (Figure 1, green), and we begin to discern some apparently larger discrepancies between DFT and LFMM. For Y = H_2O and Y = H^- the models are qualitatively different, but we note that these ligands also have the largest deviations for the homoleptic complexes (see Table 2). The absolute structures compare reasonably well (Figure 2), and had the LFMM Pt−OH_2 distance in $[Pt(OH_2)_4]^{2+}$ been within the "normal" 0.02 Å tolerance of the DFT value, a qualitatively correct picture would have resulted.

A summary of the type of data shown in Figure 1 is shown in Table 3, but for each ligand X in PtX_3Y. Root mean square

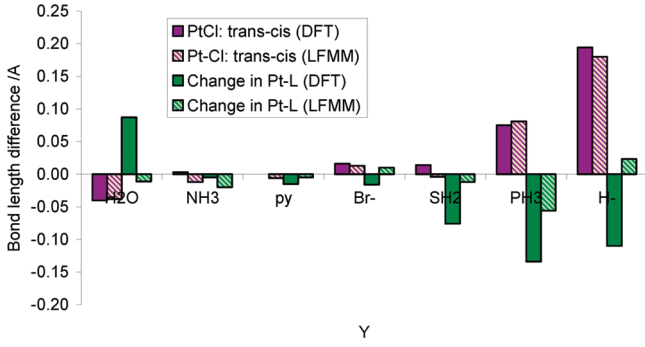

Figure 1. Difference in cis and trans Pt−Cl bond lengths in [$Pt^{II}Cl_3Y$] (in purple) and change in Pt−Y bond length in [$Pt^{II}Cl_3Y$] compared to the homoleptic species [$Pt^{II}Y_4$] (green).

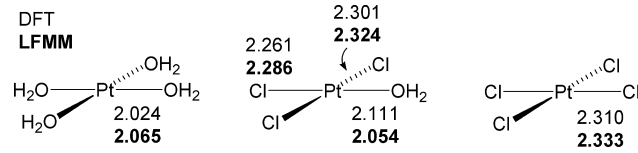

Figure 2. Calculated structural data for selected Pt complexes.

Table 3. RMSD (per Ligand Type) of Absolute Change in Pt−X Bond Lengths (Δ*r*(X)) and Relative *cis*−*trans* Bond Length Differences ($r(X_c) - r(X_t)$, in italics) between DFT and LFMM Structures of [PtX_3Y] and RMSD Values for Change in Pt−Y Bond Lengths (Δ*r*(Y))

X	$\Delta r(X)_{rmsd}$ $\{r(X_c) - r(X_t)\}_{rmsd}$	$\Delta r(Y)_{rmsd}$
H_2O	0.031/*0.030*	0.055
Cl	0.014/*0.011*	0.048
NH_3	0.019/*0.020*	0.037
pyridine	0.019/*0.021*	0.022
Br	0.017/*0.026*	0.058
SH_2	0.027/*0.038*	0.023
PH_3	0.026/*0.035*	0.035
H	0.028/*0.027*	0.058

deviations for the absolute difference in Pt−X and Pt−Y distances are shown and indicate that LFMM is reliably able to predict the Pt−X distances in PtX_3Y complexes. The Pt−Y distances are less accurate, partly due to the effect described above and partly to the fact the LFMM is not always able to predict the full extent of the trans influence. For example, $[PtH_3(NH_3)]^-$ is calculated to have a Pt−N distance of 2.153 Å by DFT, but only 2.082 Å by LFMM. However, both values represent a significant elongation of the Pt−N bond length compared to that found in $[Pt(NH_3)_4]^{2+}$.

Also included in Table 3 are the rms DFT and LFMM deviations between the cis and trans bond lengths. These are all low, indicating that the LFMM gets the balance between the cis and trans influence correct when the cis and trans groups are chemically the same.

Thus, the LFMM gets the right sense but not the full magnitude of the trans influence, at least compared to DFT. A further example is shown in Figure 3 for $[Pt(py)_3Y]$. DFT often gives substantially greater changes in Pt−Y distances than LFMM, particularly for H^-. One potential source of this difference is that each ligand has a single set of LFMM parameters. To the extent that the trans influence is a competition between two ligands such that as one binds more strongly the other weakens, we might anticipate that the AOM parameters in each case should be adjustable to reflect the changing nature of the bonding.[37] This is akin to the idea of a polarizable force field, where the partial atomic charges are variable as opposed to a fixed set. Having multiple sets of AOM parameters also parallels the VALBOND-TRANS idea of explicitly modifying a given ligand's parameters as a function of the trans ligand and would certainly improve matters, as would any increase in the number of parameters, and is an idea for future development. Meanwhile, the current model is qualitatively correct, although we note that increasingly strong trans influences are expected to be increasingly hard for the LFMM model to get right.

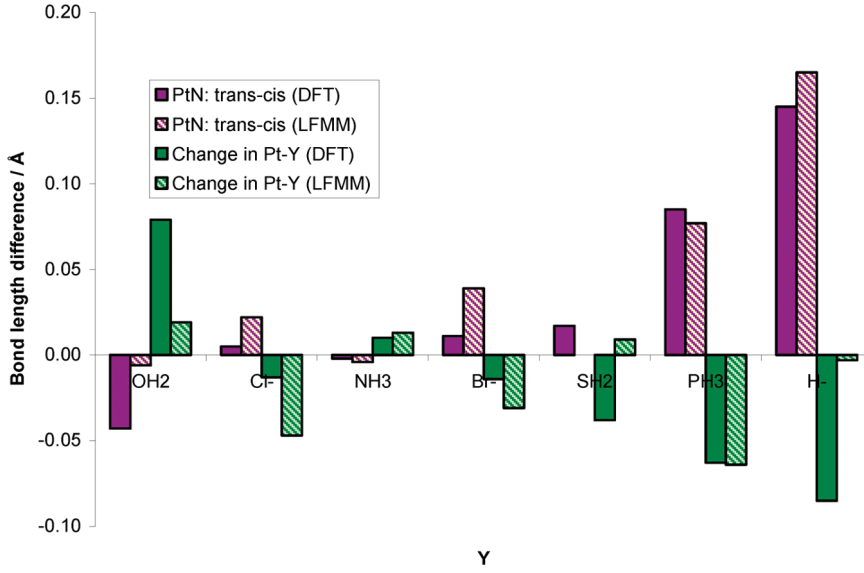

Figure 3. Cis−trans Pt−N difference and change in Pt−Y bond length for [$Ptpy_3Y$].

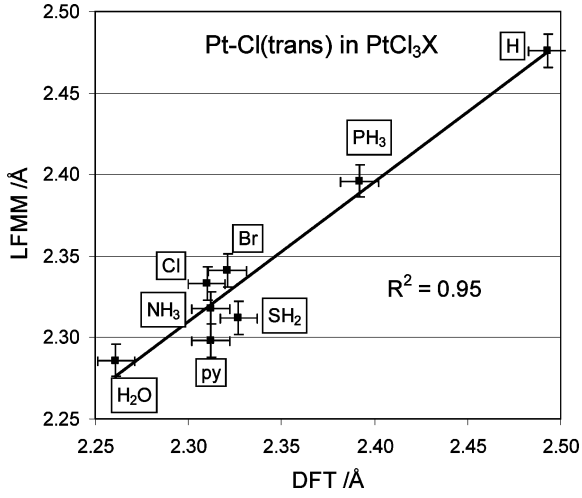

Figure 4. Correlation between computed trans Pt−Cl distances (Å) in [$PtCl_3X$] complexes. Error bars are 0.01 Å.

This issue with the very largest trans influences is not the only problem, since it would not seem to account for H_2O and SH_2, which have apparently fairly modest trans influences and yet some of the biggest errors. The chemical difference between these ligands and the others considered here is their ability to engage in strong intramolecular hydrogen bonding, although how this is related to the errors we observe is unclear.

For the simple ligands considered so far, the following order of decreasing trans influence is obtained:

LFMM: $H^- > PH_3 > SH_2 > Br^- > Cl^-$, pyridine, $NH_3 > H_2O$

DFT: $H^- > PH_3 > SH_2$, Br^-, pyridine, NH_3, $Cl^- > H_2O$

Both the DFT and LFMM data are consistent with experiment, although, as shown graphically in Figure 4, DFT does not significantly differentiate between SH_2, Br^-, pyridine, NH_3, and Cl^-.

PtX_2Y_2. For PtX_2Y_2 complexes we can compare both structural and energetic features: (a) relative Pt−X bond lengths in the cis and trans species, (b) relative Pt−Y bond lengths in the cis and trans species, and (c) relative energies of the cis and trans complexes (compared to the energies determined by DFT).

PtX_2Y_2 Geometries. It is harder to assess the performance of individual parameters for different ligands in PtX_2Y_2 because both the Pt−X and Pt−Y parameters have an effect on the geometry. However, general trends can be observed, and overall there is good agreement between DFT and LFMM.

Again, the chloro complexes $PtCl_2Y_2$ are used to illustrate the performance of the DFT and LFMM calculations. Figure 5 shows how the Pt−Cl and Pt−Y bond lengths differ in $PtCl_2Y_2$ complexes. The qualitative correlation is good, and where there is disagreement ($Y = NH_3$ or SH_2), the difference between cis and trans bond lengths is small. The relative Pt−Y distances are generally also qualitatively correct, but as noted for $PtCl_3Y$ species, the differences between LFMM and DFT are larger for Pt−Y than for Pt−Cl, although here the offending ligand appears to be PH_3, to which we will return.

A summary of the type of information shown in Figure 5 is collected for all PtX_2Y_2 complexes in Table 4. The Pt−PH_3 parameters consistently give poorer rmsd values for the Pt−P cis−trans values, while Pt−H parameters have a large rmsd value for the Pt−Y cis−trans values. However, the latter is in part due to the consistently large trans influence of the hydride ligand such that the apparently bigger deviations are actually a relatively minor proportion of the total change. As shown in Figure 6, the LFMM is always qualitatively correct.

PtX_2Y_2 Energies. The relative energies of the cis and trans isomers depend on several factors. Of course, both forms are usually synthetically accessible, since by exploiting the trans effect, kinetic products can be trapped. The higher energy form is metastable, provided there is a high enough barrier to cis−trans interconversion.

Generally, in the gas phase the trans isomer is by DFT lower in energy, especially if one of the ligands is formally

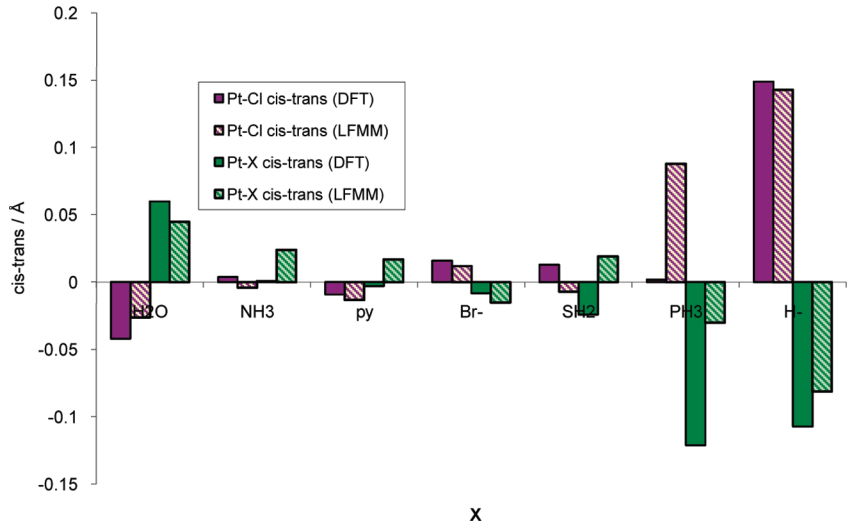

Figure 5. Difference in cis and trans Pt−Cl and Pt−X bond lengths in $[PtCl_2X_2]$.

Table 4. RMSD for Absolute Bond Lengths (Roman Text) and Difference in Cis and Trans Bond Lengths (Italic Text) for $[PtX_2Y_2]$

	rmsd	
X in PtX_2Y_2	$Pt-X_c-Pt-X_t$	$Pt-Y_c-Pt-Y_t$
H_2O	0.038/*0.039*	0.032/*0.039*
Cl	0.026/*0.034*	0.028/*0.041*
NH_3	0.027/*0.022*	0.019/*0.016*
pyridine	0.029/*0.022*	0.016/*0.020*
Br	0.022/*0.030*	0.027/*0.022*
SH_2	0.030/*0.037*	0.030/*0.029*
PH_3	0.044/*0.048*	0.034/*0.038*
H	0.020/*0.019*	0.048/*0.046*

anionic. Given the size of the ligands considered so far, steric effects play only a small role in determining the cis−trans preference. Electrostatics play a much larger role and is the main reason for the trans isomer being preferred, since this minimizes unfavorable ligand−ligand electrostatic repulsions. The trans influence is also important and should favor cis structures as the ligand with the stronger trans influence is opposite the weaker one. Solvation also plays a crucial role in determining the relative stabilities of the isomers. The cis isomer is preferred due to its larger dipole moment (compared to the zero overall dipole moment in the trans isomer).[5] The dipole will be especially large for complexes where X is formally anionic while Y is formally neutral.

The calculated energy differences between cis and trans PtX_2Y_2 species are compared in Figure 7. We have used the lowest energy isomer in each case. The DFT energies may include a solvation correction (DFT^S) or exclude solvation (DFT^{GP}). In either case, the COSMO-optimized structure was employed ($\varepsilon = 78.4$). The LFMM solvation correction ($LFMM^S$) employs the solvation energy computed via the Poisson−Boltzmann scheme as implemented in MOE.

Ideally, we would like a linear correlation between LFMM and DFT energy differences, with a gradient of 1 and an intercept of 0 plus no points in the top left and bottom right quadrants. While this is generally true for the gas phase energies, there are examples where DFT predicts the cis isomer to be more stable and LFMM predicts it to be less stable, and vice versa. When implicit solvent is included, the qualitative predictions of the more stable isomer improve, especially in the "cis" regime, although occasionally LFMM stabilizes the cis isomer too much compared to the DFT results. The worst cases are indicated by the arrows in Figure 7 and involve hydride or PH_3.

Generally, inclusion of solvent stabilizes the cis isomer relative to the trans isomer and the data points tend to move down and to the left. This is due to the presence of a dipole moment in the cis, but not trans, isomer.[5] There are a few anomalous complexes for which this does not happen, i.e., solvation stabilizes trans instead of cis. All of these include water, SH_2, or hydride as ligands. For water and SH_2, the dipole moment of the complex is dependent on the orientation of the hydrogen atoms and this will affect the degree of stabilization afforded by solvation. Additionally, the gas-phase energies are recorded at the solvated geometries. For water and SH_2, the preferred orientation of the ligands may be different at the gas-phase geometries, altering the relative energies. The Pt−H bond lengths may also be affected by the presence of a solvent and be different in the gas phase. In the LFMM calculations more trans structures are stabilized by solvation relative to their cis isomers than for DFT, although some are common to both methods. Again these often include aqua or SH_2 ligands, although not so much hydride ligands. Additionally pyridine ligands show this trend.

Pt−PH_3: A Special Case? The simple phosphine ligand, PH_3, stands out as being particularly poorly treated. On the one hand, this could be considered insignificant, since PH_3 is never used synthetically. On the other hand, PH_3 is a perfectly acceptable computational model and given we are comparing to DFT calculations, we had no a priori reason to expect such a failure. In addition, we have always adopted a "one size fits all" philosophy for am(m)ines; i.e., we use a single set of M−N LFMM parameters for all NR_3 donors.

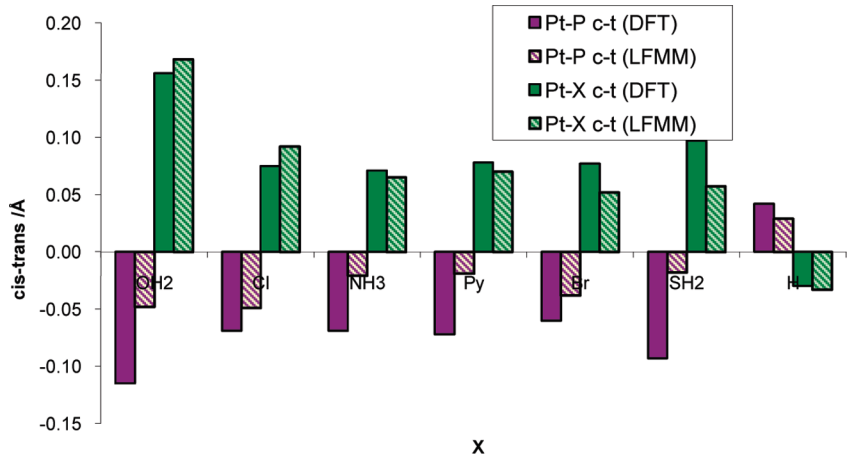

Figure 6. Relative cis and trans geometries of $[PtH_2X_2]$.

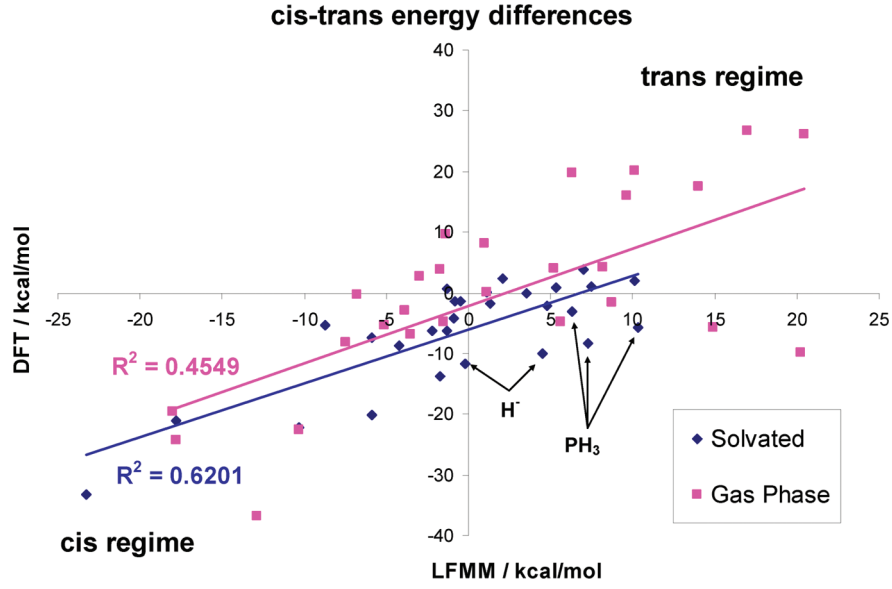

Figure 7. Relative energies of cis and trans isomers/kcal mol^{-1} ($E_{cis} - E_{trans}$). The raw data upon which this figure is based are included in the Supporting Information, Table S5.

We anticipated using the $Pt-PH_3$ LFMM parameters for all $Pt-PR_3$ moieties.

Phosphine does have some qualitatively different features with respect to the other ligands considered here. It is the only π-acceptor ligand in the set, plus its homoleptic complex is one of the few for which the CHelpG analysis suggested a net negative charge on the metal center. We therefore experimented with modifying the partial charges but without significant effect. Finally, we simply replaced PH_3 with PMe_3 and repeated the DFT and LFMM analysis with the same LFMM parameters (Figure 8). Curiously, with solvation corrections added, this "cured" two of the three problem cases such that only one point (dark blue diamonds in Figure 8) is in an incorrect quadrant.

As shown in Figure 9, the geometric comparison of $[Pt(PMe_3)_2X_2]$ is also good. The only complex with cause for concern is $[Pt(PMe_3)_2(py)_2]^{2+}$, where the comparison of both the gas and solution phase relative energies remains less satisfactory, even though the structures appear fine.

$[Pt(PMe_3)_3X]$. The geometries of $[Pt(PMe_3)_3X]$ complexes from LFMM and DFT optimizations are compared in Figure 10. In all cases, except H^-, DFT and LFMM are in agreement. For H^-, if we consider absolute bond lengths, there is only a 0.04 Å difference between the two methods. The large discrepancy in the change in bond length is attributed to the too short Pt−H bond length in the homoleptic species optimized using LFMM.

$[Pt(PMe_3)X_3]$. The geometries of $[Pt(PMe_3)X_3]$ complexes from LFMM and DFT optimizations are compared in Figure 11. In all cases, DFT and LFMM results are in agreement about whether the cis or trans Pt−X bond length should be longer and also about whether the Pt−P bond length has increased or decreased relative to that found in the homoleptic species.

In summary, the LFMM parameters developed on the basis of PH_3 work very well for PMe_3 species.

Other Systems. Having developed a set of LFMM parameters for Pt(II) complexes, we can now explore the

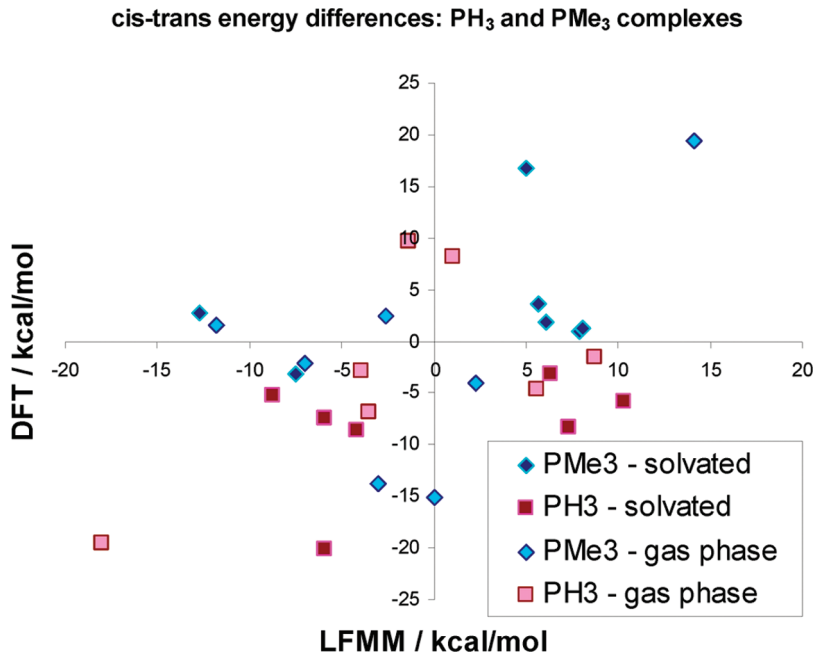

Figure 8. Cis−trans energy difference (kcal/mol) for $[Pt(PR_3)_2X_2]$ complexes, R = H, CH_3. The raw data are included in Supporting Information, Table S6.

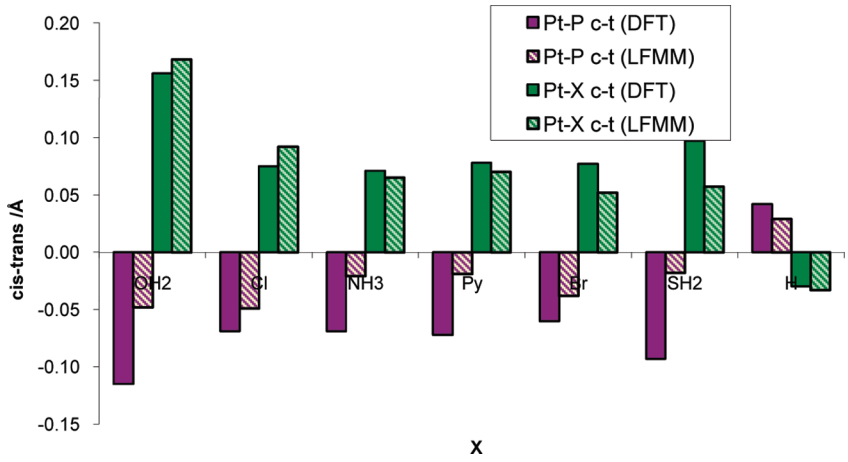

Figure 9. Relative cis and trans geometries of $[Pt(PMe_3)_2X_2]$.

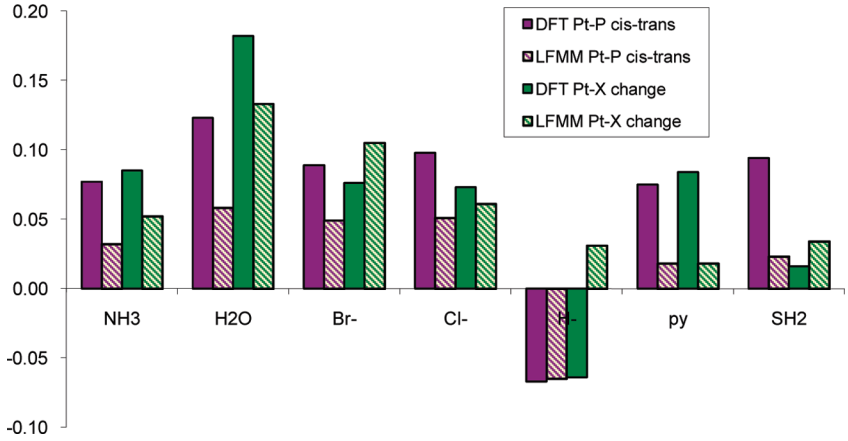

Figure 10. Comparison between DFT and LFMM geometries of $[Pt(PMe_3)_3X]$.

model's performance for species not used in the training set. For example, Rappé et al. have reported UFF calculations for *cis*-dibromo(1,2-diaminocyclohexane)platinum(II), and we compare their results with ours in Table 5.

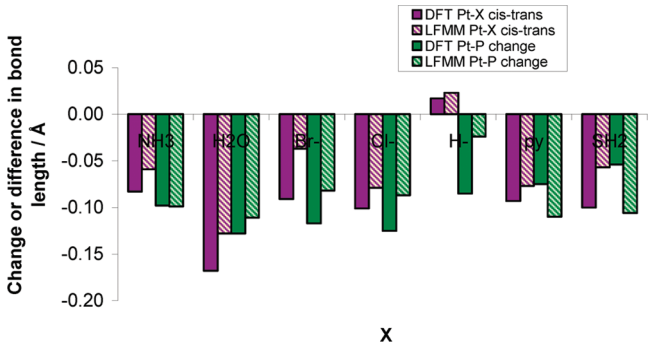

Figure 11. Comparison of DFT and LFMM relative bond lengths (cis−trans) or change in bond length (Pt−P compared to the homoleptic bond length).

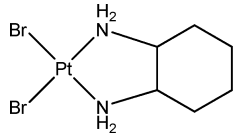

LFMM reproduces the crystal structure and DFT structure well, and performs somewhat better than UFF in terms of the Pt−Br distance and the Br−Pt−Br angle.

Further comparisons were made. Four examples of $[PtX_3Y]$ complexes were located in the Cambridge Structural Database[35] and a comparison of the experimentally derived Pt−L distances with those computed by LFMM (and DFT for $[PtH(PMe_3)_3]^+$) is presented in Table 6.

In each case, the relative bond lengths of X_{cis} and X_{trans} are correct, although LFMM tends to generate somewhat longer Pt−P bonds than observed. Note that due to the crystallographic difficulties of estimating H−Pt bond lengths, no comment is offered on the LFMM versus experimental Pt−H bond length comparisons.

A similar comparison with experiment but for $[PtXYZ_2]$ systems is shown in Table 7. Again, LFMM tends to give slightly too long Pt−L contacts, but the qualitative agreement is good.

We next explore the effect of increasing the bulk of the substituents on NR_3 and PR_3 systems. Increasing the steric bulk of the ligands causes the geometry around the metal to distort from square planar toward tetrahedral. The AOM parameters used in the LFMM calculations have to be flexible enough to allow this distortion.

DFT calculations of $[Pt(PR_3)_4]^{2+}$ (R = H, Me, Et) show a progressive distortion from square planar toward tetrahedral. The large L−Pt−L angle changes from 180° to 157.2° to 149°.[51] A crystal structure is available for $[Pt(PEt_3)_4]^{2+}$ that supports the DFT calculations, and LFMM calculations reproduce the trends predicted by DFT.

Table 6. Comparison of Selected Experimental Structures with LFMM Structures for Complexes $[PtX_3Y]$*

Ref	Structure	LFMM (DFT) bond lengths / Å	Experimental bond lengths / Å	
39,40	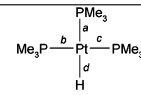	*a*: 2.423 (2.367) *b*: 2.334 (2.302) *c*: 2.334 (2.302) *d*: 1.637 (1.625)	*a*: 2.323 *b*: 2.287 *c*: 2.293 *d*: *	*a*: 2.315 *b*: 2.289 *c*: 2.299 *d*: 1.922
41	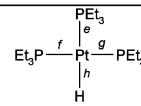	*e*: 2.384 *f*: 2.312 *g*: 2.312 *h*: 1.624	*e*: 2.335/2.291 *f*: 2.297/2.286 *g*: 2.304/2.308 *h*: */*	
42	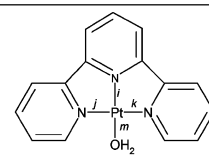	*i*: 1.917 *j*: 2.046 *k*: 2.053 *m*: 2.085	*i*: 1.914 *j*: 2.009 *k*: 2.021 *m*: 2.040	
43	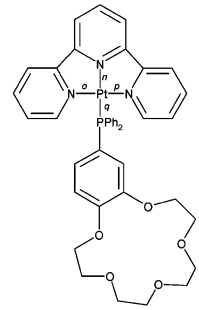	*n*: 1.999 *o*: 2.097 *p*: 2.073 *q*: 2.287	*n*: 2.003 *o*: 2.081 *p*: 2.073 *q*: 2.232	

* Pt−H distance not reported.

For R = Me and Et, stochastic LFMM conformational searches were carried out and the lowest energy PtL_4 isomers are included in Table 8. The tetrahedral distortion tends to be larger for DFT structures than for LFMM but both show a significant change from planar coordination. For R = Me, there is a DFT structure that is much closer to the LFMM result and only 1.3 kcal mol^{-1} higher than the most stable isomer. The tetrahedral distortion thus seems to be a relatively low-energy mode and relatively large variations in the P−Pt−P angles are associated with relatively small changes in energy.

For R = Et, the steric demands are even greater. A crystal structure of the ClO_4^- salt of this complex is available, and both DFT and LFMM are in good agreement with it.[51] An overlay of the LFMM, DFT, and crystal structures is shown in Figure 12. There is some variation in the orientation of some of the ethyl groups, but this is not energetically significant.

A more interesting, if unexpected, result is that the LFMM stochastic searches for $[Pt(PEt_3)_4]^{2+}$ locate a second structural

Table 5. Comparison of Experimental and Computed Geometries of *cis*-Dibromo(1,2-diaminocyclohexane)platinum(II)

	Expt[38]	UFF	LFMM	DFT
Pt−Br/Å	2.434	2.519	2.414	2.456
Pt−N/Å	2.056	2.040	2.036	2.036
Br−Pt−Br/deg	95.61	89.9	97.5	93.2
N−Pt−N/deg	83.5	87.4	86.9	82.3
N−Pt−Br (cis)/deg	89.0/91.9		87.8	92.4/92.1
planarity (Br−Pt−N)/deg	175.4/172.4	underestimated by 6°	174.7/174.7	174.7/174.5

Table 7. LFMM-Optimized and Experimental Bond Lengths for Structures of the Formula $[PtXYZ_2]$*

ref	Structure	LFMM geometry / Å	Experimental Geometry / Å
44-46	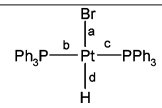	a: 2.604 b: 2.361 c: 2.361 d: 1.582	a: 2.523/2.535/2.516 b: 2.283/2.275/2.279 c: 2.283/2.281/2.286 d:1.610/1.592/*
47	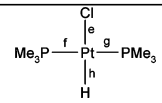	e: 2.482 f: 2.307 g: 2.307 h: 1.575	e: 2.423 f: 2.281 g: 2.281 h: *
48	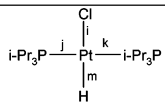	i: 2.497 j: 2.342 k: 2.332 m: 1.586	i: 2.395 j: 2.286 k: 2.287 m: 1.868
49	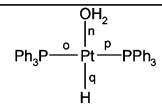	n: 2.319 o: 2.307 p: 2.310 q: 1.566	n: 2.182/2.191/2.186 o: 2.295/2.291/2.294 p: 2.279/2.285/2.287 q:1.420/1.586/1.612
50	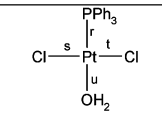	r: 2.257 s: 2.339 t: 2.327 u: 2.159	r: 2.248/2.238 s: 2.329/2.309 t: 2.341/2.358 u: 2.131/2.118

* Pt−H distance not reported.

Table 8. Geometries of $[Pt(PR_3)_4]^{2+}$ for R = H, Me, Et[a]

$[Pt(PH_3)_4]^{2+}$	DFT	LFMM
Pt−P/Å	2.324	2.290
P−Pt−P trans/deg	180.0	180.0
P−Pt−P cis/deg	90.0	90.0

$[Pt(PMe_3)_4]^{2+}$	DFT	LFMM
Pt−P/Å	2.348(2.360)	2.348
P−C/Å	1.824(1.824−1.826)	1.845−1.854
P−Pt−P trans/deg	143.5(157.2)	161.4
P−Pt−P cis/deg	95.6(92.2)	91.5
Pt−P−C/deg	110.0−126.3(113.6−120.7)	118.2−122.0

$[Pt(PEt_3)_4]^{2+}$	DFT	LFMM	experiment[51]
Pt−P/Å	2.365−2.396	2.384−2.409	2.330−2.351
P−C/Å	1.843−1.864	1.771−2.213	1.839−1.931
P−Pt−P trans/deg	145.2−146.9	158.3−158.9	150.4−151.0
P−Pt−P cis/deg	93.6−96.5	91.5−92.4	93.3−94.2
Pt−P−C/deg	105.0−131.2	101.9−129.2	106.5−127.3

[a] For R = Me, the DFT data in parentheses correspond to a structure 1.3 kcal mol^{-1} higher than the overall minimum.

type with one phosphine dissociated. Using DFT, this lies 6.5 kcal mol^{-1} higher in energy than the tetracoordinated structure, but LFMM predicts it to be the more stable form. This arises because the present LFMM parametrization did not include any energetic information that would discriminate these two situations. Our study of $[M(OH_2)_6]^{2+}$ complexes demonstrates that the LFMM can be designed to reproduce such energy differences.[52] Moreover, that study and the current one shows that the use of a Morse function to describe the M−L bond stretching potential allows the LFMM model to support arbitrarily long M−L bond lengths

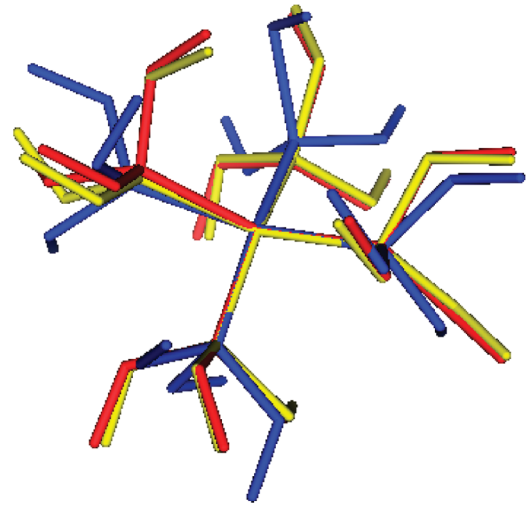

Figure 12. Overlay of optimized geometries of $[Pt(PEt_3)_4]^{2+}$ from DFT (red), LFMM (blue), and a crystal structure (yellow).

Table 9. Selected Bond Lengths (Å) and Angles (deg) for $[Pt(NR_3)_4]^{2+}$ Complexes, R = H, Me

$[Pt(NH_3)_4]^{2+}$	DFT	LFMM
Pt−N	2.035	2.047
N−Pt−N_{trans}	180.0	179.3
N−Pt−N_{cis}	90.0	90.0

$[Pt(NMe_3)_4]^{2+}$	DFT		LFMM	
Pt−N1	2.217	2.258	2.233	2.263
Pt−N2	2.225	2.258	2.232	2.263
Pt−N3	2.260	2.258	2.285	2.263
Pt−N4	2.267	2.258	2.283	2.263
N2−Pt−N3	97.4	95.3	97.1	94.5
N1−Pt−N2	97.4	95.3	96.9	94.5
N1−Pt−N3	138.6	144.4	138.4	147.5
N1−Pt−N4	97.4	95.3	97.1	94.5
N2−Pt−N4	138.0	144.4	138.6	147.5
N3−Pt−N4	96.9	95.3	97.7	94.5

without exacting an infinite energy penalty. That is, the LFMM can effectively describe M−L bond breaking. We will return to this issue in a future publication.

For $[Pt(NR_3)_4]^{2+}$ complexes, the steric influence of R on the geometry around Pt^{II} is also very large, even more so than for the phosphine counterparts. Upon replacing NH_3 with NMe_3 ligands, the steric repulsion is increased so much that, in addition to the tetrahedral distortion found for the PMe_3 system, the Pt−N bond lengths increases by ∼0.2 Å in both DFT and LFMM optimizations, whereas the comparable Pt−P distance was largely unaffected (Table 9). This is consistent with platinum being a soft metal that therefore forms stronger bonds to second-row donors such as phosphines.

Two DFT minima for $[Pt(NMe_3)_4]^{2+}$ have been located, lying only 0.3 kcal mol^{-1} apart. The less stable structure has C_{4h} symmetry and the other is slightly distorted from this. LFMM also finds both these minima and predicts that they lie 1.8 kcal mol^{-1} apart in energy with the symmetric structure being more stable, although this energy difference is small and probably within the error limits of the calcula-

Table 10. Structures and Energies (with respect to symmetric structure in kcal mol^{-1}) of $[Pt(NEt_3)_4]^{2+}$

$[Pt(NEt_3)_4]^{2+}$	DFT	LFMM	LFMM, no bond but charges unadjusted	no bond, charges adjusted
E: isomer 1	(−42.7) −47.7	−8.2 (−7.8)	−22.9 (−23.3)	−15.2 (−7.9)
Pt−N1	2.105	2.178	2.143	2.145
Pt−N2	2.175	2.186	2.202	2.200
Pt−N3	2.148	2.187	2.204	2.201
Pt−N4	5.454	4.702	5.422	4.785
N2−Pt−N3	151.8	156.9	155.1	155.4
N1−Pt−N2	102.8	101.8	102.2	102.0
N1−Pt−N3	105.5	101.2	102.7	102.5
E: isomer 2	(−36.6) −41.9	−8.8 (−7.1)	−9.8 (−9.3)	−17.5 (−9.9)
Pt−N1	2.094	2.122	2.128	2.131
Pt−N2	2.175	2.211	2.205	2.203
Pt−N3	2.149	2.188	2.186	2.179
Pt−N4	5.607	6.251	6.249	5.916
N2−Pt−N3	153.2	156.7	156.9	159.9
N1−Pt−N2	100.8	101.7	101.4	101.5
N1−Pt−N3	106.0	101.3	101.4	101.3
E: isomer 3	(−30.3) −34.8	+4.7 (+4.9)	−11.6 (−10.6)	−2.6 (+4.1)
Pt−N1	2.110	2.186	2.155	2.156
Pt−N2	2.162	2.166	2.179	2.177
Pt−N3	2.152	2.209	2.228	2.225
Pt−N4	5.065	4.642	6.584	4.781
N2−Pt−N3	153.6	158.1	156.8	156.8
N1−Pt−N2	103.6	99.2	100.2	100.1
N1−Pt−N3	102.5	102.1	102.9	102.9

tions. Geometries for both minima are reported in Table 9 and LFMM and DFT are in excellent agreement.

When R = Et, the steric bulk of the ligand is even greater and DFT optimizations show that one ligand spontaneously dissociates from the Pt^{2+} center, leaving an approximately T-shaped $[Pt(NEt_3)_3]^{2+}$ moiety. We have located stationary points for three of these structures, and reoptimized them using LFMM. These results are summarized in Table 10 and the overlay of the lowest energy LFMM and DFT geometries is shown in Figure 13. With care, we were able to optimize a "symmetrical" structure with DFT where all four NEt_3 ligands are coordinated. It has Pt−N bond lengths of 2.371 Å, cis angles of 95.0° and trans angles of 143.9° compared to 2.350 Å, 95.5°, and 145.8° from LFMM, respectively. The symmetrical structure lies ∼43 kcal mol^{-1} higher than the most stable tricoordinate structure in DFT and ∼9 kcal mol^{-1} higher in LFMM.

LFMM predicts slightly longer lengths than DFT, but the "sense" of which bond lengths are longer is retained, along with good comparisons between angles. Moreover, even though there is an explicit Pt−N connection in the LFMM treatment, one Pt−N distance spontaneously lengthens to more than 4.5 Å.

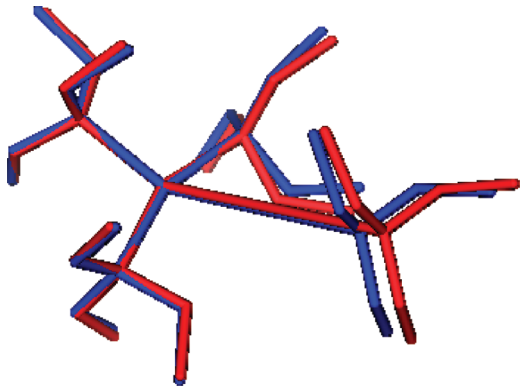

Figure 13. Overlay of LFMM (blue) and DFT (red) optimized geometries for the lowest energy forms of $[Pt(NEt_3)_4]^{2+}$.

Some improvement in the relative Pt−N bond lengths is obtained when this explicit bond between Pt and the "dissociating" amine ligand is deleted, but the change in geometry is not very large.

A search of the Cambridge Structural Database[35] did not reveal any crystal structures of either $[Pt(NEt_3)_3]^{2+}$ or $[Pt(NEt_3)_4]^{2+}$, so we are unable to comment on how this result compares to experiment.

For both the phosphine and amine systems, the LFMM parametrization did not include energetic information and its ability to treat the dissociation found for the R = Et systems is at best qualitative. Removing the explicit Pt−N bond and recalculating charges leads to apparently better energetics and a slight reduction in the $Pt-N^1$ bond length compared to the $Pt-N^{2,3}$ bond lengths. However, a reparameterization is required if an explicit treatment of bond dissociation is desired.

Finally, we return to complexes containing pyridine ligands. Our DFT orbital analysis suggests pyridine acts as a strong σ-donor and a strong π-donor toward Pt^{II}. In $[Pt(py)_4]^{2+}$, the two limiting (i.e., highest symmetry) orientations of the py planes give rise to the same LFSE (Figure 14). Hence, there is no electronic driver to determine the ligand plane orientation, and simple steric considerations suggest that the most stable arrangement is a "propellor" arrangement with the ligand planes tending to lie perpendicular to the PtN_4 coordination plane rather than in the plane where the contacts of the ortho hydrogens would be unfavorable. In practice, both experiment[53] and LFMM give propeller arrangements, although the pitch is 0° for LFMM

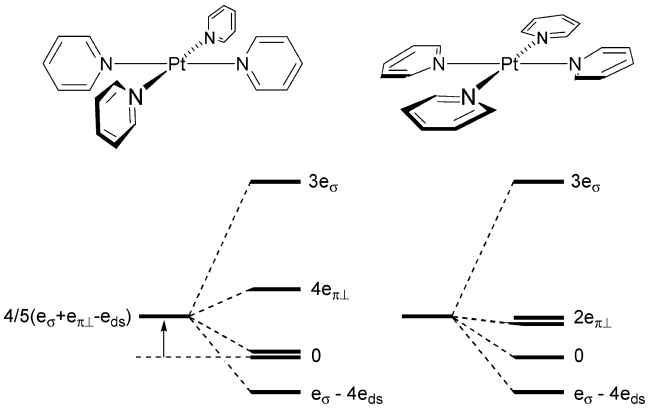

Figure 14. Limiting orientations of pyridine planes for $[Pt(py)_4]^{2+}$ and their associated d orbital energy level diagrams. Left: perpendicular orientation, propeller pitch 0°. Right: parallel orientation, pitch 90°.

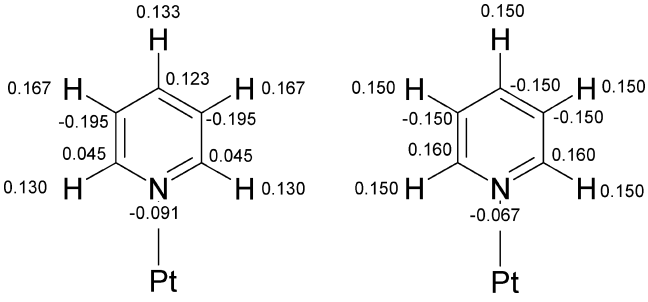

Figure 15. Charges on pyridine ring when coordinated to Pt^{II}.

but ranges from 2 to 28° in the X-ray structure of $[Pt(py)_4]Cl_2 \cdot 3H_2O$ (Figure 15).

In mixed-ligand systems, the pyridine orientation is influenced by both the coligand and solvation. For example, without solvation corrections, DFT and LFMM calculations for *trans*-$[Pt(py)_2H_2]$ and $[Pt(py)H_3]^-$ place the pyridine rings coplanar with the coordination plane due to the favorable electrostatic attraction between the positively charged ortho hydrogen atoms of the pyridine rings and the negatively charged hydrides. For *trans*-$[Pt(py)_2H_2]$, DFT predicts that the coplanar isomer is preferred by 2.7 kcal mol^{-1} and by 0.9 kcal mol^{-1} for $[Pt(py)H_3]^-$. When COSMO solvation corrections are included, the perpendicular py arrangement is preferred by 2.0 and 2.1 kcal mol^{-1} respectively.

LFMM gives a very similar picture. For $[Pt(py)H_3]^-$ without solvation, the coplanar structure is favored by 3.9 kcal mol^{-1} while with a solvation correction, the perpendicular structure is favored by 1.8 kcal mol^{-1}. For *trans*-$[Pt(py)_2H_2]$, attempts to locate the perpendicular isomer by LFMM spontaneously revert to the coplanar form. However, if the Born solvation correction is included in the optimization procedure, as opposed to being added as a single point energy correction, the pyridine rings tilt out of the coordination plane and the energy decreases by 3.8 kcal mol^{-1} relative to the coplanar form.

Conclusions

Ligand field molecular mechanics provides a good description of the trans influence in a wide range of Pt^{II} complexes. Not only can we compute good structures but the relative energies of *cis*- and *trans*-PtX_2Y_2 species virtually always agree with estimates based on DFT.

The ligand field stabilization energy (LFSE) provides a bridge between all the ligands such that variation of any one can lead to changes in all the others. The LFSE is inherently centrosymmetric but, in conjunction with the other LFMM energy terms, we can induce an asymmetric motion such that the stronger trans influenced ligand is more "anchored" and either moves toward the metal or, at the very least, retains its original bond length, while the weaker one moves away. This latter motion can be substantial. For $[PtCl_3H]^{2-}$, the trans Pt−Cl distance is elongated by nearly 0.25 Å relative to that of $[PtCl_4]^{2-}$ (Figure 4).

LFMM calculations give a decreasing trans influence series: $H^- > PH_3 > SH_2 > Br^- > Cl^-$, pyridine, $NH_3 > H_2O$. This compares well with the DFT calculated series: $H^- > PH_3 > SH_2$, Br^-, pyridine, NH_3, $Cl^- > H_2O$. Both the DFT and LFMM data are in agreement with the order reported in the literature.

The LFMM parameters developed for simple ligands also describe the behavior of their bulkier congeners. In both $[Pt(PR_3)_4]^{2+}$ and $[Pt(NR_3)_4]^{2+}$ (R = H, Me, Et), we see progressive tetrahedral distortions and even spontaneous ligand dissociation. Overall, while we are occasionally short of the full magnitude of the trans influence, in virtually every case, the LFMM is in qualitative agreement with DFT. This gives us some confidence to take the model forward to examine platinum-based anticancer agents and their interactions with biomolecules such as DNA.

Supporting Information Available: LFMM parameters, DFT geometry optimization data for $[PdCl_4]^{2-}$, $[PdBr_4]^{2-}$ and $[Pd(NH_3)_4]^{2+}$ using a wide variety of functional/solvation model combinations; cis−trans geometries and energies for $[PtCl_2(NH_3)_2]$ using OPBE with and without COSMO corrections; DFT and LFMM cis−trans energy differences for PtA_2B_2 systems with and without solvation corrections (i.e., the data used to construct Figures 7 and 8). This material is available free of charge via the Internet at http://pubs.acs.org.

Acknowledgment. A.E.A. acknowledges the award of an EPSRC fellowship and the EPSRC Chemical Database Service for access to the Cambridge Structural Database.

References

(1) Pidcock, A.; Richards, R. E.; Venanzi, L. M. *J. Chem. Soc. A* **1966**, 1707.

(2) Mason, R.; McWeeny, R.; Towl, A. D. C. *Faraday Discuss.* **1969**, *47*, 20.

(3) Pearson, R. G. *Inorg. Chem.* **1973**, *12*, 712–713.

(4) Jorgensen, C. K. *Inorg. Chem.* **1964**, *3*, 1201–1202.

(5) Harvey, J. N.; Heslop, K. M.; Orpen, A. G.; Pringle, P. G. *Chem. Commun.* **2003**, 278–279.

(6) Landis, C. R.; Cleveland, T.; Firman, T. K. *J. Am. Chem. Soc.* **1998**, *120*, 2641–2649.

(7) Deeth, R. J.; Anastasi, A.; Diedrich, C.; Randell, K. *Coord. Chem. Rev.* **2009**, *253*, 795–816.

(8) Bentz, A.; Comba, P.; Deeth, R. J.; Kerscher, M.; Seibold, B.; Wadepohl, H. *Inorg. Chem.* **2008**, *47*, 9518–9527.

(9) Deeth, R. J.; Hearnshaw, L. J. A. *Dalton Trans.* **2006**, 1092–1100.

(10) Deeth, R. J.; Foulis, D. L.; Williams-Hubbard, B. J. *Dalton Trans.* **2003**, 3949–3955.

(11) Baerends, E. J.; Autschbach, J.; Bérces, A.; Bickelhaupt, F. M.; Bo, C.; Boerrigter, P. M.; Cavallo, L.; Chong, D. P.; Deng, L.; M., D. R.; E., E. D.; van Faassen, M.; Fan, L.; Fischer, T. H.; Fonseca Guerra, C.; van Gisbergen, S. J. A.; Groeneveld, J. A.; Gritsenko, O. V.; Grüning, M.; Harris, F. E.; van den Hoek, P.; Jacob, C. R.; Jacobsen, H.; Jensen, L.; van Kessel, G.; Kootstra, F.; van Lenthe, E.; McCormack, D. A.; Michalak, A.; Neugebauer, J.; Nicu, V. P.; Osinga, V. P.; Patchkovskii, S.; Philipsen, P. H. T.; Post, D.; Pye, C. C.; Ravenek, W.; Ros, P.; Schipper, P. R. T.; Schreckenbach, G.; Snijders, J. G.; Solà, M.; Swart, M.; Swerhone, D.; te Velde, G.; Vernooijs, P.; Versluis, L.; Visscher, L.; Visser, O.; Wang, F.; Wesolowski, T. A.; van Wezenbeek, E.; Wiesenekker, G.; Wolff, S. K.; Woo, T. K.; Yakovlev, A. L.; Ziegler, T. *ADF2006.01*; SCM, Theoretical Chemistry, Vrije Universiteit: Amsterdam, The Netherlands, 2006.

(12) Guerra, C. F.; Snijders, J. G.; te Velde, G.; Baerends, E. J. *Theor. Chem. Acc.* **1998**, *99*, 391–403.

(13) Van Lenthe, E.; Baerends, E. J.; Snijders, J. G. *J. Chem. Phys.* **1994**, *101*, 9783–9792.

(14) Van Lenthe, E.; Baerends, E. J.; Snijders, J. G. *J. Chem. Phys.* **1993**, *99*, 4597–4610.

(15) Pye, C. C.; Ziegler, T. *Theor. Chem. Acc.* **1999**, *101*, 396–408.

(16) Allinger, N. L.; Zhou, X. F.; Bergsma, J. *J. Mol. Struct.* **1994**, *118*, 69–83.

(17) Bon, R. S.; van Vliet, B.; Sprenkels, N. E.; Schmitz, R. F.; de Kanter, F. J. J.; Stevens, C. V.; Swart, M.; Bickelhaupt, F. M.; Groen, M. B.; Orru, R. V. A. *J. Org. Chem.* **2005**, *70*, 3542–3553.

(18) Fan, L. Y.; Ziegler, T. *J. Phys. Chem.* **1992**, *96*, 6937–6941.

(19) Fan, L. Y.; Ziegler, T. *J. Chem. Phys.* **1992**, *96*, 9005–9012.

(20) Frisch, M. J.; Trucks, G. W.; Schlegel, H. B.; Scuseria, G. E.; Robb, M. A.; Cheeseman, J. R.; Montgomery, J., J. A.; Vreven, T.; Kudin, K. N.; Burant, J. C.; Millam, J. M.; Iyengar, S. S.; Tomasi, J.; Barone, V.; Mennucci, B.; Cossi, M.; Scalmani, G.; Rega, N.; Petersson, G. A.; Nakatsuji, H.; Hada, M.; Ehara, M.; Toyota, K.; Fukuda, R.; Hasegawa, J.; Ishida, M.; Nakajima, T.; Honda, Y.; Kitao, O.; Nakai, H.; Klene, M.; Li, X.; Knox, J. E.; Hratchian, H. P.; Cross, J. B.; Bakken, V.; Adamo, C.; Jaramillo, J.; Gomperts, R.; Stratmann, R. E.; Yazyev, O.; Austin, A. J.; Cammi, R.; Pomelli, C.; Ochterski, J. W.; Ayala, P. Y.; Morokuma, K.; Voth, G. A.; Salvador, P.; Dannenberg, J. J.; Zakrzewski, V. G.; Dapprich, S.; Daniels, A. D.; Strain, M. C.; Farkas, O.; Malick, D. K.; Rabuck, A. D.; Raghavachari, K.; Foresman, J. B.; Ortiz, J. V.; Cui, Q.; Baboul, A. G.; Clifford, S.; Cioslowski, J.; Stefanov, B. B.; Liu, G.; Liashenko, A.; Piskorz, P.; Komaromi, I.; Martin, R. L.; Fox, D. J.; Keith, T.; Al-Laham, M. A.; Peng, C. Y.; Nanayakkara, A.; Challacombe, M.; Gill, P. M. W.; Johnson, B.; Chen, W.; Wong, M. W.; Gonzalez, C.; Pople, J. A.; *Gaussian 03, Revision C.02*; Gaussian, Inc.: Wallingford CT, 2004.

(21) Ehlers, A. W.; Bohme, M.; Dapprich, S.; Gobbi, A.; Hollwarth, A.; Jonas, V.; Kohler, K. F.; Stegmann, R.; Veldkamp, A.; Frenking, G. *Chem. Phys. Lett.* **1993**, *208*, 111–114.

(22) Bush, B. L.; Bayly, C. I.; Halgren, T. A. *J. Comput. Chem.* **1999**, *20*, 1495–1516.

(23) Breneman, C. M.; Wiberg, K. B. *J. Comput. Chem.* **1990**, *11*, 361–373.

(24) Deeth, R. J.; Fey, N.; Williams-Hubbard, B. J. *J. Comput. Chem.* **2005**, *26*, 123–130.

(25) *MOE*, 2007 ed.; Chemical Computing Group, Montreal: Montreal, 2007.

(26) Norrby, P. O.; Liljefors, T. *J. Comput. Chem.* **1998**, *19*, 1146–1166.

(27) Rappe, A. K.; Colwell, K. S.; Casewit, C. J. *Inorg. Chem.* **1993**, *32*, 3438–3450.

(28) Root, D. M.; Landis, C. R.; Cleveland, T. *J. Am. Chem. Soc.* **1993**, *115*, 4201–4209.

(29) Tubert-Brohman, I.; Schmid, M.; Meuwly, M. *J. Chem. Theor. Comp.* **2009**, *5*, 530–539.

(30) Deeth, R. J.; Munslow, I. J.; Paget, V. J. *NATO ASI Ser.* **1997**, *3/41*, 77–103.

(31) Brandt, P.; Norrby, T.; Akermark, E.; Norrby, P. O. *Inorg. Chem.* **1998**, *37*, 4120–4127.

(32) Allured, V. S.; Kelly, C. M.; Landis, C. R. *J. Am. Chem. Soc.* **1991**, *113*, 1–12.

(33) Cundari, T. R.; Fu, W.; Moody, E. W.; Slavin, L. L.; Snyder, L. A.; Sommerer, S. O.; Klinckman, T. R. *J. Phys. Chem.* **1996**, *100*, 18057–18064.

(34) Burton, V. J.; Deeth, R. J.; Kemp, C. M.; Gilbert, P. J. *J. Am. Chem. Soc.* **1995**, *117*, 8407–8415.

(35) Fletcher, D. A.; McMeeking, R. F.; Parkin, D. *J. Chem. Inf. Comput. Sci.* **1996**, *36*, 746–749.

(36) Hocking, R. K.; Deeth, R. J.; Hambley, T. W. *Inorg. Chem.* **2007**, *46*, 8238–8244.

(37) Coe, B. J.; Glenwright, S. J. *Coord. Chem. Rev.* **2000**, *203*, 5–80.

(38) Lock, C. J. L.; Pilon, P. *Acta Crystallogr., Sect. B* **1981**, *37*, 45–49.

(39) Packett, D. L.; Syed, A.; Trogler, W. C. *Organometallics* **1988**, *7*, 159–166.

(40) Adams, R. D.; Barnard, T. S.; Li, Z. Y.; Zhang, L. J. *Chem. Ber. Recl.* **1997**, *130*, 729–733.

(41) Russell, D. R.; Mazid, M. A.; Tucker, P. A. *J. Chem. Soc., Dalton Trans.* **1980**, 1737–1742.

(42) Annibale, G.; Bergamini, P.; Bertolasi, V.; Bortoluzzi, M.; Cattabriga, M.; Pitteri, B. *Eur. J. Inorg. Chem.* **2007**, 5743–5751.

(43) Yam, V. W. W.; Tang, R. P. L.; Wong, K. M. C.; Lu, X. X.; Cheung, K. K.; Zhu, N. Y. *Chem.—Eur. J.* **2002**, *8*, 4066–4076.

(44) Aldridge, S.; Coombs, D.; Jones, C. *Acta Crystallogr., Sect. E* **2003**, *59*, M584−M585.

(45) Habereder, T.; Noth, H. *Appl. Organomet. Chem.* **2003**, *17*, 525–538.

(46) Sivaramakrishna, A.; Su, H.; Moss, J. R. *Acta Crystallogr., Sect. E* **2007**, *63*, M244−M245.

(47) Packett, D. L.; Jensen, C. M.; Cowan, R. L.; Strouse, C. E.; Trogler, W. C. *Inorg. Chem.* **1985**, *24*, 3578–3583.

(48) Robertson, G. B.; Tucker, P. A.; Wickramasinghe, W. A. *Aust. J. Chem.* **1986**, *39*, 1495–1507.

(49) Parkins, A. W.; Richard, C. J.; Steed, J. W. *Inorg. Chim. Acta* **2005**, *358*, 2827–2832.

(50) Rath, N. P.; Fallis, K. A.; Anderson, G. K. *Acta Crystallogr., Sect. C* **1993**, *49*, 2079–2081.

(51) Kozelka, J.; Luthi, H. P.; Dubler, E.; Kunz, R. W. *Inorg. Chim. Acta* **1984**, *86*, 155–163.

(52) Deeth, R. J.; Randell, K. *Inorg. Chem.* **2008**, *47*, 7377–7388.

(53) Wei, C. H.; Hingerty, B. E.; Busing, W. R. *Acta Crystallogr., Sect. C* **1989**, *45*, 26.

CT9001569